Numerical Bound State Electron Dynamics of Carbon Dioxide in the Strong-Field Regime

Stanley M. Smith,[†,‡] Dmitri A. Romanov,[‡,§] Xiaosong Li,[∥] Jason A. Sonk,[⊥] H. Bernhard Schlegel,[⊥] and Robert J. Levis*[,†,‡]

Department of Chemistry, Department of Physics, and Center for Advanced Photonics Research, Temple University, Philadelphia, Pennsylvania 19122, Department of Chemistry, University of Washington, Seattle, Washington 98195, and Department of Chemistry, Wayne State University, Detroit, Michigan 48202

Received: May 15, 2009; Revised Manuscript Received: January 5, 2010

Time-dependent Hartree−Fock simulations for a linear triatomic molecule (CO_2) interacting with a short IR (1.63 eV) three-cycle pulse reveal that the carrier-envelope shape and phase are the essential field parameters determining the bound state electron dynamics during and after the laser−molecule interaction. Analysis of the induced dipole oscillation reveals that the envelope shape (Gaussian or trapezoidal) controls the excited state population distribution. Varying the carrier envelope phase for each of the two pulse envelope shapes considerably changes the excited state populations. Increasing the electric field amplitude alters the relative populations of the excited states, generally exciting higher states. A windowed Fourier transform analysis of the dipole evolution during the laser pulse reveals the dynamics of state excitation and in particular state coupling as the laser intensity increases.

Introduction

The excitation of atoms and diatomics in strong laser fields has been well-studied with respect to ionization and the generation of high harmonics[1−8](HHG). The initial process in the strong-field excitation of atoms, diatomics, and polyatomic molecules is the coupling of the laser field to the electrons in the system. The laser−molecule interaction and the ensuing electron dynamics during the pulse determine the outcome of the excitation, ionization, and rescattering processes. Tunnel and multiphoton ionization and high harmonic generation are determined by the electron dynamics during the pulse while bond breaking and bond making processes are determined by the coupled electron−nuclear dynamics during and after the laser pulse. When laser pulses are long compared to the period of the carrier wave (on the order of 10 or more optical cycles), the response of the system typically does not depend on the carrier envelope phase[9] (CEP), the difference between the peak of the carrier wave and the peak of the electric field envelope. If the excitation pulse becomes shorter, on the order of five or less cycles, the CEP can dictate the outcome of the laser−matter interaction.[10−13] Increasingly, experiments have focused on more efficiently creating high harmonics with ultrashort pulses on the order of two to five optical cycles.[14]

In the intense-pulse regime, the effect of CEP has been studied for short, few-cycle pulses. When such a few-cycle laser pulse interacts with an atomic gas, the carrier envelope phase can affect several laser-induced processes,[11,15,16] including ionization,[17,18] above-threshold ionization[19−22] (ATI), higher harmonic generation,[23,24] as well as photoelectron angular distribution.[19,21,25−30] The CEP effects for ionization are manifested by spatial asymmetries in the ionization signal along the laser polarization direction which has been attributed to electric field asymmetries. For stereo-ATI, the asymmetries in the left-right photoelectron spectra are the result of the spatially redirected tunneling to the right or left as determined by the carrier envelope phase. CEP has been shown to red-shift the HHG cutoff for H atom and has theoretically been used to control the directional rescattering to ensure that the electron only rescatters from the ion core on the side from which tunneling occurred. Both linear and circular polarized laser pulses lead to strong CEP-dependent left-right asymmetries of photoelectrons. Most of these studies have been performed on atoms or small diatomic molecules.

The interaction of short, few-cycle laser pulses has been used to explore nonadiabatic electron excitation in larger molecules theoretically.[31−33] The conjugated hydrocarbons explored in such numerical investigations exhibited an increase in nonadiabatic excitation with increasing length, however, the smallest molecules in these studies, ethylene and benzene, also exhibited nonadiabatic excitation. Molecules in the range between diatomics and ethylene offer a unique opportunity to explore nonadiabatic excitation for several classes of molecules. One class, linear triatomic molecules, represents a next step in the progression beyond diatomics. One of the most widely studied linear triatomic molecules is CO_2. The combined nuclear−electron wave packet dynamics of CO_2 has been studied for short (<200 fs) pulses using the field-following time-dependent adiabatic state approach.[34−36] In the few-cycle pulse regime for CO_2, the electron dynamics are the main contributor to any excitation processes since there is not sufficient time for the nuclear motion to occur. The electron dynamics for pulses on the order of a few cycles and the effect of CEP have not been studied for CO_2.

Here, we incorporate nonadiabatic and multielectron effects into the theoretical description of the strong-field excitation of CO_2. We seek to investigate carrier envelope shape and carrier envelope phase effects on the bound state electron dynamics occurring during strong-field excitation. We use time-dependent Hatrtee−Fock theory to investigate the interaction of a few-cycle strong-field laser pulse with the molecule as a first step to analyzing attosecond time duration bound state electron

* To whom correspondence should be addressed.
[†] Department of Chemistry, Temple University.
[‡] Center for Advanced Photonics Research, Temple University.
[§] Department of Physics, Temple University.
[∥] Department of Chemistry, University of Washington.
[⊥] Department of Chemistry, Wayne State University.

10.1021/jp904549d
Published on Web 01/29/2010

dynamics. We do not include ionization in the calculation, and thus, this investigation provides the theoretical machinery to perform time-dependent calculations in the bound state manifold, as well as a first look at possible manifestations of CEP-dependent nonadiabatic effects in strong fields. We first investigate the bound state excitation profiles by Fourier transforming the residual dipole moment oscillations for Gaussian and trapezoidal pulse shapes. Next we study the effects of carrier envelope phase on both pulse shapes using the same Fourier transform method. Finally, we use a windowed Fourier transform to reveal the nonlinear electron dynamics that occur during the few-cycle laser pulse.

Method

To investigate the bound state electron dynamics during the interaction of shaped light pulses with molecules, we employ the time-dependent Hartree−Fock (TDHF) equations. In an orthonormal basis, these equations can be written in terms of the Fock matrix, **F**, and the one-electron density matrix, **P**.

$$i\frac{\mathrm{d}\mathbf{P}(t_i)}{\mathrm{d}t} = [\mathbf{F}(t_i), \mathbf{P}(t_i)] \tag{1}$$

The Fock matrix depends not only on the time-dependent electric field, $\mathbf{E}(t)$, but also on the time-dependent density matrix. Efficient integration of this equation has been described previously.[37] The property commonly used to analyze the electron response to the laser field is the instantaneous dipole moment given by

$$\mu(t_i) = \sum Z_A R_A - tr(\mathbf{D}'\mathbf{P}'(t_i)) \tag{2}$$

where Z_A is the charge on atom A, R_A is the distance of atom A from the center of the coordinate system, $\mathbf{D}'$ is the dipole moment integral in the atomic orbital (AO) basis, and $\mathbf{P}'$ is the density matrix in the AO basis.

To simulate the response of the electrons to a short laser pulse, two field envelope shapes were used. The first envelope was Gaussian and the resulting electric field was

$$\boldsymbol{E}(t) = E_{\max}\exp\left(\frac{-t^2}{2\alpha^2}\right)\sin(\omega t + \varphi) \tag{3}$$

where α is related to the full width at half-maximum (fwhm) (fwhm = 2 α (2 ln 2)$^{1/2}$). As an example of a more complex pulse, the second pulse envelope shape investigated was trapezoidal: $|\mathbf{E}(t)|$ increased linearly to reach the value $|\mathbf{E}_{\max}|$ at the end of the first cycle, remained at $|\mathbf{E}_{\max}|$ for one cycle, and then decreased linearly to zero by the end of the next cycle.

$$\begin{aligned}
&\boldsymbol{E}(t) = (\omega t/2\pi)\mathbf{E}_{\max}\times \sin(\omega t + \phi) && \text{for } 0 \le t \le 2\pi/\omega\\
&\boldsymbol{E}(\mathrm{t}) = \mathbf{E}_{\max}\times \sin(\omega t + \phi) && \text{for } 2\pi/\omega \le t \le 4\pi/\omega\\
&\boldsymbol{E}(\mathrm{t}) = (3 - \omega t/2\pi)\mathbf{E}_{\max}\times \sin(\omega t + \phi) && \text{for } 4\pi/\omega \le t \le 6\pi/\omega\\
&\boldsymbol{E}(t) = 0 && \text{for } t < 0 \text{ and } t > 6\pi/\omega
\end{aligned} \tag{4}$$

All of the electric fields were numerically integrated to verify that the total area of each pulse was zero within the limits of numerical noise. For example, the pulse areas of the Gaussian and trapezoidal pulse in Figure 1c are 0.0012 and −0.00006, respectively. Electron dynamics in the field were simulated using the development version of the GAUSSIAN[38] series of programs with the addition of the unitary transform time-dependent Hartree−Fock algorithm (UT-TDHF).[37] Calculations were performed at the HF level of theory using aug-cc-pVTZ[39,40] basis set for carbon dioxide. At the HF/aug-cc-pVTZ level of theory for ground state CO_2, the equilibrium C−O bond distance is 1.1363 Å, which is comparable to the experimentally measured bond length of 1.162 Å.[41] The corresponding excited states from linear response time-dependent Hartree−Fock theory with transition dipoles along the molecular axis are listed in Table 1. The integrations were carried out for 24 fs with a step size of 0.0012 fs (0.05 au).

Due to the neglect of correlation effects in the Hartree−Fock Hamiltonian, the values of the excitation energies are approximations. While these calculations may not represent the exact nonadiabatic bound state electron dynamics of CO_2, these calculations do reveal important characteristic changes in nonadiabatic electron dynamics for a polyatomic molecule as a function of intense laser pulse envelope shape, carrier envelope phase, intensity ramping time to the maximum electric field, and total pulse duration. In addition, the calculations reveal important coupling mechanisms and strong field effects that occur at high, nonresonant laser intensities.

The presence of the residual dipole moment oscillations (the oscillations that continue after the laser pulse) implies the effects of nonadiabatic excitation, or nonresonant deposition of energy from the field into the molecule. Accordingly, characteristic results of this nonadiabatic excitation processes may be revealed by Fourier transforming the residual dipole oscillations. The obtained power spectrum reflects the composition of the nonadiabatic multielectron excitation in terms of the field-free states. All Fourier transforms of the residual dipole moments were calculated after the pulse, over the interval from 12 to 24 fs. The height of each peak in the Fourier transform will be referred to as the Fourier amplitude or amplitude. All Fourier transforms performed in this work were discrete Fourier transforms. The Nyquest frequency for each transform was determined, and the oversampling was calculated to be ≥6.

The Fourier transform of the residual dipole moment oscillations is an important tool for analyzing the excited states that become populated during the pulse, but the dynamics of excitation is equally important in understanding nonadiabatic processes. The instantaneous state of the excitation can be assessed by the time-dependent excitation volume, the area under the absolute Fourier transform taken over a relatively short interval. Tracing the evolution of the excitation volume may yield some insight into the electron dynamics during the pulse. A windowed Fourier transform (WFT) can be used for this purpose and is formally defined as

$$F(t,\omega) = \int f(s)\mu(s - t)e^{is\omega}\,\mathrm{d}s \tag{5}$$

where $f(s)$ is the window shape from eq 3 or 4, t is the time step used to move $f(s)$ through the instantaneous dipole moment $\mu(t)$ defined in eq 2. The shape of the window is the same as the pulse envelope shape and the maximum height of the window is the same as maximum height of the envelope of the instantaneous dipole moment. The overlap of the dipole moment

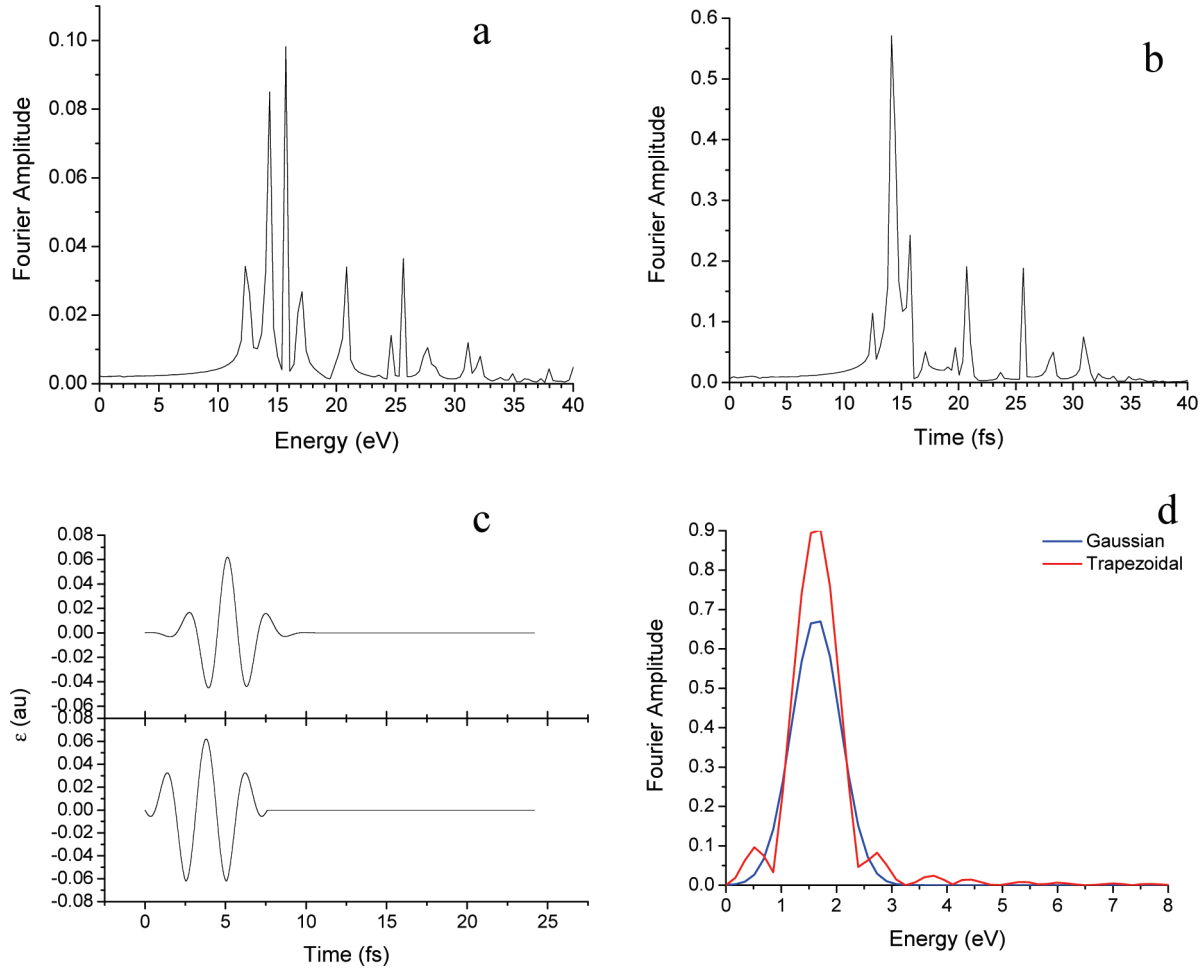

Figure 1. Fourier transforms of the residual dipole moment oscillations of CO_2 for pulse parameters of $I = 1.1 \times 10^{14}$ W/cm^2, $\omega = 0.06$ au with (a) Gaussian envelope, (b) trapezoidal envelope, (c) Gaussian (top) and trapezoidal (bottom) electric field profile, and (d) the Fourier transform (spectrum) of the Gaussian and trapezoidal pulses.

TABLE 1: Excited-State Energies and Transition Dipole Moments along the Molecular Axis

transitions along the molecular axis with nonzero transition dipoles (TDHF coefficient)	energy (eV) from TDHF	oscillator strength	transition dipole moment
HOMO−1 → LUMO+1 (0.47)	12.36	0.0785	0.5069
HOMO → LUMO+2 (0.47)			
HOMO−1 → LUMO+9 (0.41)	14.30	0.97	1.67
HOMO → LUMO+8 (0.41)			
HOMO−4 → LUMO (0.56)	15.72	0.33	0.93
HOMO−4 → LUMO+7 (0.27)			
HOMO−1 → LUMO+11 (0.42)	16.93	0.044	0.32
HOMO → LUMO+12 (0.42)			
HOMO−5 → LUMO+3 (0.42)	19.16	0.001	0.05
HOMO−4 → LUMO+4 (0.49)			
HOMO−3 → LUMO+6 (0.42)	19.77	0.033	0.26
HOMO−2 → LUMO+5 (0.42)			
HOMO−4 → LUMO + 1 (0.31)	20.20	0.23	0.69
HOMO−4 → LUMO+7 (0.48)			
HOMO−5 → LUMO+3 (0.49)	20.73	0.14	0.53
HOMO−4 → LUMO+4 (0.36)			
HOMO−1 → LUMO+18 (0.44)	20.95	0.021	0.20
HOMO → LUMO+17 (0.44)			
HOMO−5 → LUMO+10 (0.66)	23.57	0.033	0.24
HOMO−5 → LUMO+15 (0.58)	24.59	0.030	0.22
HOMO−4 → LUMO+16 (0.24)			
HOMO−4 → LUMO+16 (0.46)	25.64	0.56	0.98
HOMO−4 → LUMO+21 (0.31)			

and the window function increases to a maximum (i.e., the point where the maximum of the window and the maximum of the envelope of the dipole moment coincide or $\Delta\tau = 0$) and then decreases. This WFT technique is similar to the sliding window transform[42,43] used in the analysis of wave packet dynamics.

Results and Discussion

We are concerned with those characteristics of the intense laser pulse that are potentially effective in controlling nonadiabatic processes such as carrier envelope phase, amplitude, and shape. In an intense, few cycle pulse, the envelope changes so rapidly that a large number of excited states of a molecule are considerably Stark-shifted and momentarily engaged, so that attribution of particular excitation volume features to excitation dynamics may be a challenge. In our analysis we address this concern. First, we analyze the spectral composition of the residual dipole oscillations to reveal the effects of the envelope amplitude profile and phase shift on the cumulative excitation of the molecule. Second, we analyze the time-dependent excitation profile using a windowed Fourier transform to explore the details of nonadiabatic bound state electron dynamics in the molecule during the pulse. We will investigate the effects of pulse shape (Gaussian or trapezoidal), carrier envelope phase, maximum electric field, and ramping time to the maximum electric field on the excitation spectra to determine how these parameters possibly control nonadiabatic excitation in our target molecule.

a. Postpulse Dipole Oscillations: Cumulative Effects of Carrier Envelope Shape and Phase. Figure 1 shows the response of the residual dipole moment of CO_2 to a short, intense

pulse with the electric field polarized along the molecular axis. Figure 1a displays the Fourier transform of the residual dipole moment oscillations for a Gaussian-envelope pulse (shown in the top panel of Figure 1c and described by eq 3) with an intensity $I = 1.1 \times 10^{14}$ W/cm^2, fwhm = 3.5 fs, and a field frequency of 0.06 au which corresponds to a photon energy of 1.63 eV. The first peak in Figure 1a can be ascribed to the lowest lying excited state of CO_2 that is 12.4 eV at the HF/aug-cc-pVTZ level of theory. Since the photon energy is not resonant with this first excited state or any excited state at this level of theory the Fourier transform of the residual dipole moment oscillations reveals the nonadiabatic excitation spectrum. The second and third peaks are at 14.3 and 15.6 eV. Excited states above the ionization potential (13.77 eV)[44] are most accurately described by continuum states;[45−47] however continuum states are not included in these calculations because we are focusing on excitation, not ionization. All excited states of CO_2 are predissociative.[48] Since the states at 14.3, 15.6, and 16.7 eV are embedded in the continuum, electron excitation proceeding through these states can possibly be viewed as a precursor to ionization. For all the three excited states, the transition dipole moments with the ground state lie parallel to the molecular axis; the state-to-state transition dipoles lie in the same direction.

To investigate the effect of a simple change in pulse envelope on the excitation spectrum, we compare the Gaussian shape to a trapezoidal shape. Figure 1b shows the excitation spectrum for a trapezoidal pulse, shown in the bottom panel of Figure 1c and described by eq 4, with the same values for peak field intensity and carrier frequency as in Figure 1a. Comparison of parts a and b of Figure 1 reveals several significant differences in the excitation spectra. The first difference concerns the position and amplitude of the maximum spectral peak. The excitation by the Gaussian pulse (Figure 1a) results in a maximum Fourier amplitude of 0.098 for the 15.6 eV feature. Excitation using the trapezoidal pulse results in the maximum Fourier amplitude of 0.58 for the feature at 14.3 eV; this is approximately six times larger than the maximum feature excited by the Gaussian pulse. Second, the amplitudes of the minor peaks for the Gaussian pulse are 0.035 for the 12.4 eV state and 0.084 for the 14.3 eV state, while the minor peak amplitudes for the trapezoidal pulse are much larger: 0.12 for the 14.3 eV state and 0.30 for the 15.6 eV state. Similar increases in the Fourier amplitudes of the 20.95 and 25.64 eV peaks are also observed for the trapezoidal pulse in comparison with the Gaussian pulse. Thus, the change in envelope shape has a significant effect both on the overall peak amplitudes and on the identity of the largest peak.

There are three possible explanations for the effect of the pulse envelope on the excitation spectrum: the difference in the total integrated energy, the different patterns of the electric field maxima per half cycle, and the spectral bandwidth of the Gaussian and trapezoidal pulses. The integrated energy of a pulse can be approximated by

$$\text{energy} \approx \frac{\varepsilon_0}{2} \int_0^\tau |E(t)|^2 \, dt \qquad (6)$$

where τ is the effective pulse duration, $|E(t)|$ is the absolute value of the electric fields shown in Figure 1c, and ε_0 is the permittivity of free space. For the pulse parameters used in Figure 1, the integrated energy in the Gaussian pulse is 0.168 au while the integrated energy for the trapezoidal pulse is 0.271 au, 38% greater. The absolute values of the maximum electric field per laser half-cycle have a broader distribution for the

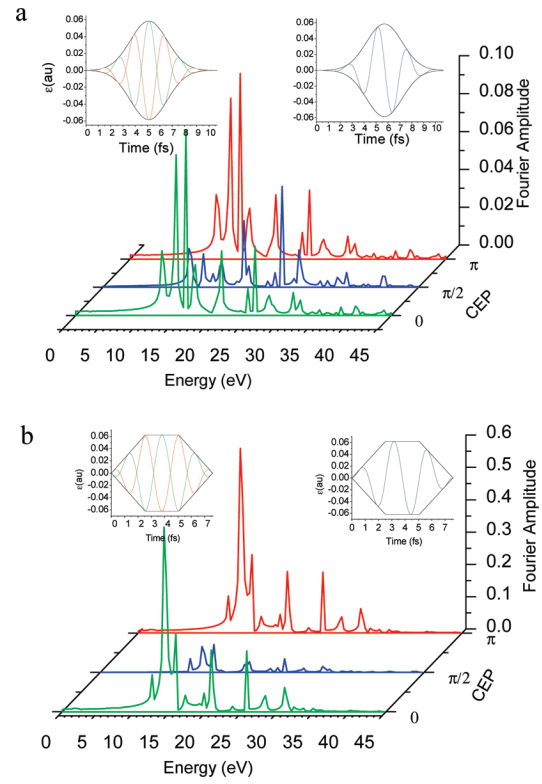

Figure 2. The Fourier transforms of the residual dipole moment oscillations for CO_2 at an intensity of 1.1×10^{14} W/cm^2, $\omega = 0.06$ au for carrier envelope phases of $\phi = 0$, $\pi/2$, and π for (a) Gaussian and (b) trapezoidal pulse shapes. (Note: The insets are the applied electric fields.)

trapezoidal pulse (0.002, 0.038, 0.062, 0.062, 0.062, 0.038, and 0.002 au) than for the Gaussian pulse (0.005, 0.018, 0.047, 0.062, 0.047, 0.018, and 0.005 au). Figure 1d shows the spectrum of the electric field for both the Gaussian and trapezoidal pulse shapes. The spectral bandwidth is nearly the same for both electric fields; however, the electric field of the trapezoidal pulse shape reveals several oscillations in the sideband resulting from the hard cut off of the electric field. Thus, any of these major differences in the pulse shape may be the cause of the differences in the excited state spectra observed in parts a and b of Figure 1.

To clarify whether the maximum electric field per laser half-cycle or the integrated energy controls the excitation spectrum, we investigated the effect of the carrier envelope phase (CEP) on the residual excitation spectrum. Changing CEP alters the pattern of electric field maxima much more than the integrated pulse energy. A comparison of the residual excitation for CEP values of $\phi = 0$, $\pi/2$, and π, is shown in Figure 2. In this comparison, the intensity and frequency values are identical to those used in Figure 1. The excitation spectrum shown in Figure 2a reveals that when $\phi = \pi/2$ the peak amplitudes are approximately 5 times smaller than those in the spectra with $\phi = 0$ and π phases (as expected, the latter two spectra are the same). At the chosen CEP values, the Gaussian pulses have integrated energy of 0.168 au compared to an integrated energy of 0.271 au for the trapezoidal pulses. Since the integrated energy is constant as a function of CEP, the changes are not due to the integrated pulse energy. The maximum absolute electric field values, for the Gaussian envelope, decrease by approximately 10% for $\phi = \pi/2$ (0.056 au) in comparison with $\phi = 0$ (0.062 au), and the value of the least maximum experiences an even larger decrease, about 40%. The spectrum

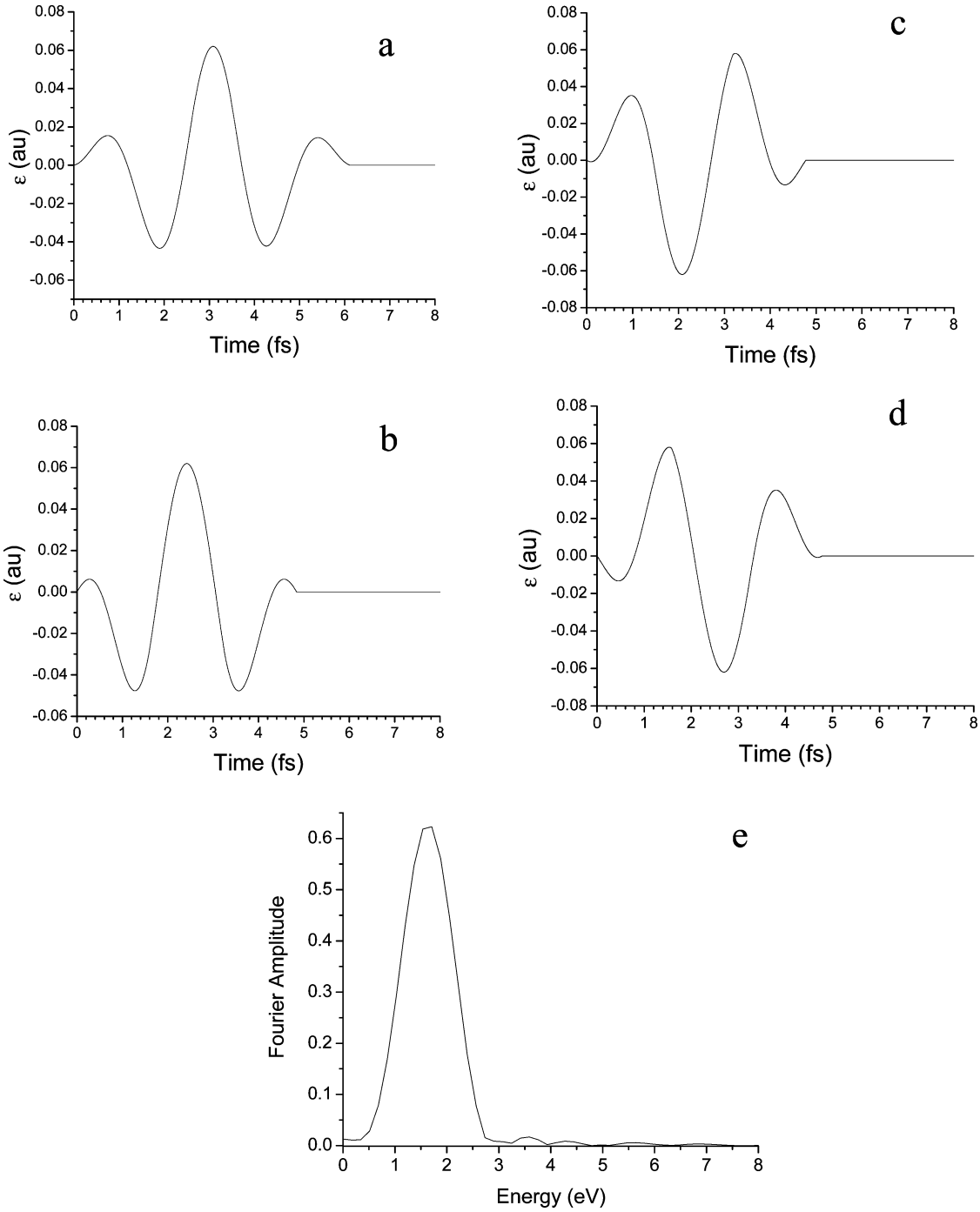

Figure 3. The electric field profiles for a trapezoidal pulse with a photon energy of $\hbar\omega = 1.63$ eV, and an intensity $I = 1.1 \times 10^{14}$ W/cm^2: (a) a ramping time of 2.6 fs, a total pulse duration of 6.02 fs, and a phase $\phi = 0$; (b) a ramping time of 1.57 fs, a total pulse duration of 4.79 fs, and phase $\phi = 0$; (c) a ramping time of 1.57 fs, a total pulse duration of 4.79 fs, and phase $\phi = 3\pi/4$; (d) time inversion of the pulse in (c); (e) the Fourier transform (spectrum) of the electric field of (a).

of the electric field is the same for all phases of the Gaussian pulse. Thus, we conclude that the difference in the excited state spectrum must primarily be due to the half cycle maxima of the electric field experienced by the molecule as determined by the electronic structure approximation that we use for CO_2.

The hypothesis that the residual excitation spectrum is controlled by the pattern of electric field maxima per half cycle experienced by the molecule is further supported by the data for the CEP dependence for the trapezoidal pulse shown in Figure 2b. Again the residual excited state spectra for $\phi = 0$ (or π) have much greater amplitudes in comparison with $\phi = \pi/2$. For the trapezoidal pulse, at $\phi = 0$ and π, the maximum field is reached three times while at $\phi = \pi/2$ the maximum electric field is attained only twice. For the Gaussian pulse at $\phi = 0$, π the maximum electric field (0.062 au) is only reached once, at the center of the pulse. At $\phi = \pi/2$ the maximum electric field, determined by the envelope maximum, is never reached. The excitation spectrum in Figure 2b, at $\phi = \pi/2$, has peak amplitudes approximately 6.7 times smaller than those in the spectra at $\phi = 0$ and π phases (as expected, the latter two spectra are the same). These changes are not due to the integrated pulse energy because the integrated pulse energies are identical. The electric field maxima per half cycle for $\phi = 0$ or π and $\phi = \pi/2$ changes; however, contrary to the Gaussian

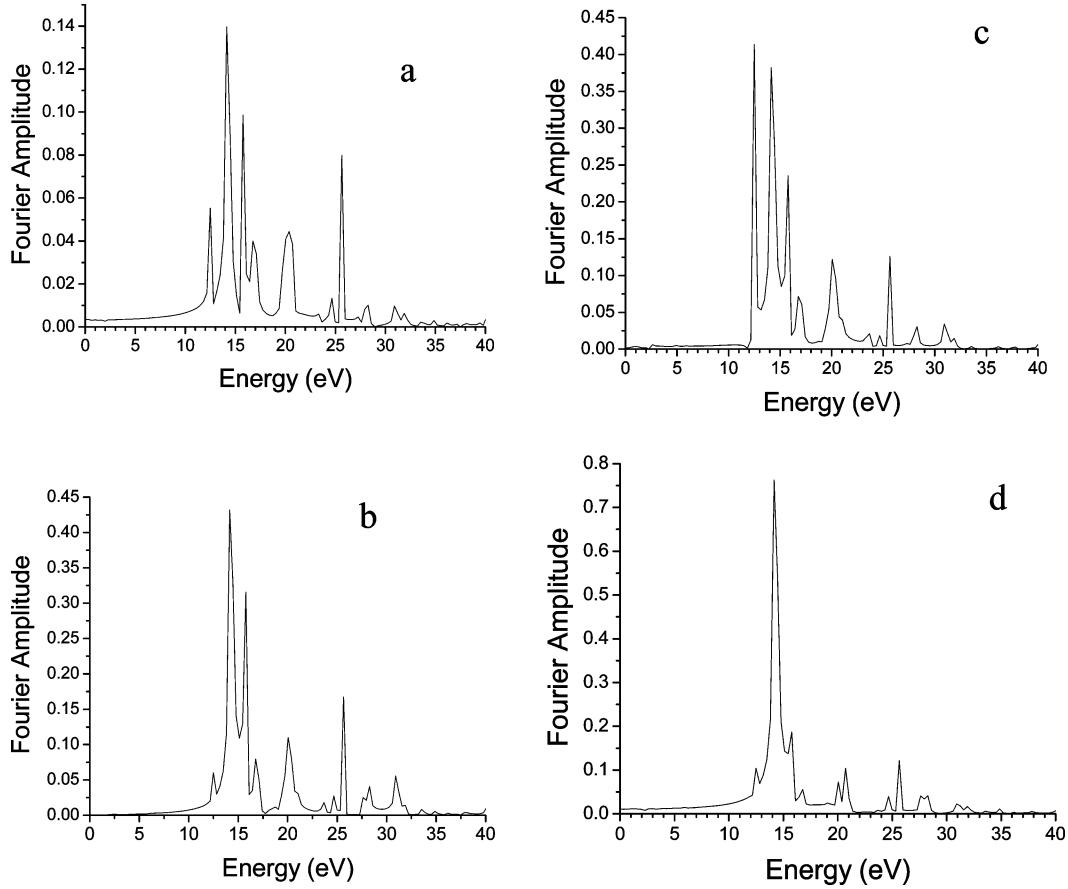

Figure 4. The Fourier transforms of the residual dipole moment oscillations for the electric fields of (a) Figure 3a, (b) Figure 3b, (c) Figure 3c, and (d) Figure 3d.

case, the highest maximum remains constant while the smallest maximum drops to zero. Again, the spectrum of the electric field is the same for all phases of the trapezoidal pulse. These changes are similar to those for the Gaussian pulse shape supporting the assertion that the difference in excited state spectra is primarily due to the pattern of the half cycle maxima of electric field given the level of our approximation to CO_2.

To explore the differences between the Gaussian and trapezoidal pulse in greater detail, the ramping time and pulse duration were varied for the trapezoidal pulse while keeping the integrated energy nearly constant for a series of pulses. Figure 3a shows the electric field for a trapezoidal pulse when the ramping time is 2.6 fs, the total pulse duration is 6.02 fs, and the integrated energy is 0.16794 au for a carrier frequency of 0.06 au and maximum electric field amplitude of 0.062 au. These field parameters were chosen so that the ramp approximates the steepest ramp of the Gaussian pulse, the integrated energies are approximately the same (0.16794 au for the trapezoidal pulse shape and 0.16788 au for the Gaussian) and the maximum electric field is reached only once during the pulse. The electric field for the trapezoidal envelope shown in Figure 3a and that for the Gaussian envelope in Figure 1c are nearly identical. The corresponding electric field spectra are shown in Figure 3e (for Figure 3a) and Figure 1d. These figures show that the bandwidth is nearly the same for both pulse shapes while the electric field spectrum in Figure 3d exhibits small side bands. The corresponding excitation spectrum for the electric field in Figure 3a is shown in Figure 4a and reveals a nonadiabatic excitation spectrum that is similar to the spectrum in Figure 1a. The main difference is in the Fourier amplitude of the 14.3 eV peak: 0.139 for the trapezoidal pulse and 0.085 for the Gaussian pulse. The similarity of the excitation spectra of Figures 1a and 4a (i.e., the 12.4 and 25.6 eV peaks are ~2 times larger in Figure 4 than in Figure 1, while the 15.6 and ~20 eV peaks have nearly the same amplitude in both figures) makes the excitation spectrum of Figure 4a appear to be a partial combination of both the trapezoidal and Gaussian pulses. This suggests that the small side bands in the electric field spectrum of Figure 3a (shown if Figure 3e) have little or no effect on the excitation spectrum and that either the ramping time or half-cycle maxima in the pulse produce the observed changes in the excitation spectra. To explore which property of the pulse is dominant, the ramping time was decreased to 1.57 fs, decreasing the pulse duration to 4.79 fs, while maintaining both the integrated energy, 0.1679 au for Figure 3b and 0.1683 au for Figure 3c, and the number laser half-cycle maxima in the pulse. The difference between these two fields is the CEP, $\phi = 0$ for Figure 3b and $\phi = 3\pi/4$ for Figure 3c. This CEP difference affects the pattern of the electric field maxima per half cycle in the pulse. Parts b and c of Figure 4 show the corresponding excitation spectra for these two pulses. The first noticeable difference is the Fourier amplitude of the largest feature. For both CEPs, the largest feature has a Fourier amplitude of approximately 0.43, suggesting that ramping the field more rapidly may have the expected effect of increasing the nonadiabatic excitation. The pulse with a CEP of $3\pi/4$ reaches the maximum electric field in ~2 fs, and this is shorter than the field with a CEP of 0 (~2.5 fs). Ramping more quickly to E_{max} appears to make the pulse nonadiabtically couple more efficiently to the 12.4 eV state which has a smaller transition dipole.

As a final test of the CEP effect, time reversal was applied to the electric field in Figure 3c as shown in Figure 3d. The maximum electric field occurs at ~2.9 fs, while the distribution of the electric field maxima, the integrated energy, pulse duration, and spectral pulse shape (Fourier transform of $E(t)$)

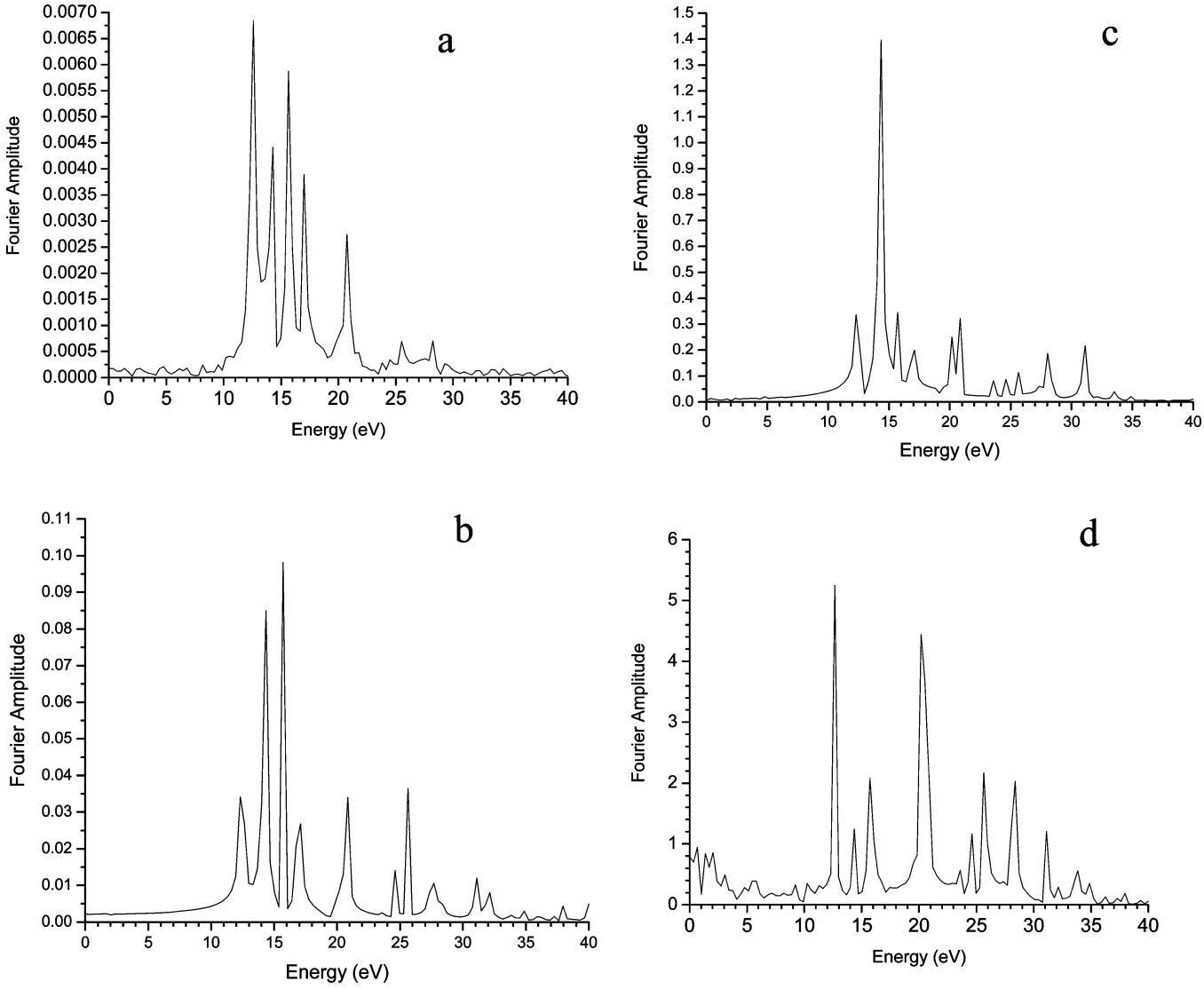

Figure 5. The Fourier transforms of the residual dipole moment oscillations for CO_2 for a Gaussian pulse with a frequency $\omega = 0.06$ au and $\phi = 0$ with intensities (a) 8.75×10^{13}, (b) 1.1×10^{14}, (c) 2.5×10^{14}, and (d) 5.0×10^{14} W/cm^2.

all remain the same. Figure 4d shows the resulting excitation spectra for this pulse. The most noticeable difference between parts c and d of Figure 4 is the 0.78 Fourier amplitude of the 14.3 eV state in Figure 4d. This Fourier amplitude is greater than the amplitude for the same state shown in Figure 2b where the pulse duration was longer, ~7.5 fs, with a greater integrated energy of 0.271 au. This suggests that the factors controlling nonadiabatic excitation cannot be separated. The ramping time, pulse duration, and CEP all collectively control the electric field maxima per half cycle and thus affect the excitation outcome.

To further explore the effects of the electric field amplitude on the excited state spectra, the maximum electric field was varied for a Gaussian pulse, while the carrier frequency, fwhm, and carrier envelope phase were held constant at $\omega = 0.06$ au 3.5 fs, and $\phi = 0$, respectively. In Figure 5a, $I = 8.75 \times 10^{13}$ W/cm^2 and the three largest peaks are observed at energy 12.4, 14.3, and 15.6 eV with amplitudes of 0.0069, 0.0044, and 0.0058 respectively. This excited state spectrum is similar to that for $\phi = \pi/2$. The intensity for Figure 5b is $I = 1.1 \times 10^{14}$ W/cm^2 and the amplitudes of the same three peaks are 0.035, 0.086, and 0.098. Thus, the excitation spectrum has changed appreciably and the 15.6 eV peak now has the largest amplitude. Figure 5c shows the excitation spectrum when the intensity is $I = 2.5 \times 10^{14}$ W/cm^2. The amplitudes of the same three peaks have increased to 0.34, 1.4, and 0.35, with the 14.3 eV peak having the largest amplitude. At $I = 5.0 \times 10^{14}$ W/cm^2, the excited state spectrum shown in Figure 5d reveals that the largest amplitudes now belong to the 12.4, 15.6, and 20.7 eV features with corresponding amplitudes of 5.2, 2.1, and 4.4, respectively. The general conclusion is that the excited state with the largest amplitude changes as a function of intensity.

Increasing intensity in Figure 5 causes an increase in the excitation volume (the overall area under the Fourier transform). The change in excitation volume may be explained by nonadiabatic multielectron excitation theory (NME),[49−52] which describes the probability to make a transition from the ground state, $|g\rangle$, to some excited state, $|Ex\rangle$, per laser half-cycle as

$$P_{|g\rangle \rightarrow |Ex\rangle} = \exp\left[\frac{-\pi\Delta_0}{4\hbar\omega E_0\sqrt{\mu^2 + \frac{\alpha_g{}^*\Delta_0}{4}}}\right] \qquad (7)$$

where Δ_0 is the energy difference between the two states, ω is the laser frequency, E_0 is the maximum magnitude of the electric field, μ is the transition dipole moment between the two states, and $\alpha_g{}^*$

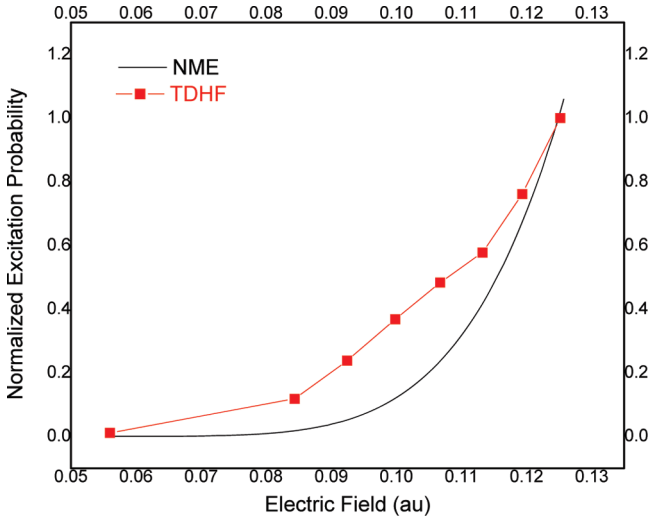

Figure 6. A comparison of the NME excitation probability to the THDF integrated excitation for a Gaussian pulse shape with constant fwhm and phase $\phi = 0$.

is the dynamic polarizability of the ground state with the contribution of the Δ_0 state removed. The most recent version of NME theory[51,52] extends a two-state, single active electron (SAE) model to a multielectron model through inclusion of the dynamic polarizability. The three key steps summarizing this model include: (i) nonadiabatic absorption of energy resulting in an electron gaining ponderomotive energy (defined as $U_p = e^2\varepsilon_o^2/4m_e\omega^2$); (ii) formation of a quasi-continuum in the excited electronic state manifold; and (iii) coupling to a doorway state in the quasi-continuum. The electron ponderomotive energy increases in parallel with the formation of the quasi-continuum. Once the ponderomotive potential is equal to Δ_0, the electron makes the transition to the doorway state and continues to quickly climb through the quasi-continuum, experiencing classical plasma-like energy absorption. This leads to either an excited or ionized molecule after interaction with the laser pulse. As in the case of transition to a true continuum, the total excitation probability is obtained by summation of the conditional probabilities over half-cycles of the laser pulse. By the mth half-cycle of the pulse, the total excitation probability for a neutral molecule is

$$P_{\text{total}}^{\text{neutral}}(m) = 1 - \prod_{n=1}^{m}[1 - P_{|g\rangle\rightarrow|DS\rangle}(n)] \qquad (8)$$

where the dependence $P_{|g\rangle\rightarrow|DS\rangle}(n)$ on the cycle number, n, is determined by the envelope of the laser pulse. NME theory suggests that a higher intensity electric field should have a greater excitation probability than a lower intensity electric field. The bound state electron dynamics described in this paper are consistent with NME theory. The present calculations demonstrate an increase in excitation volume with increasing laser intensity in agreement with the NME model and further reveal how the excitation volume is distributed over the field-free excited states as a function of increasing intensity. Figure 6 shows a comparison of the NME excitation probability with the integrated excitation volume for eight different intensities. The deviation of the TDHF curve from the NME may due to several factors; however, two are most probable. The first factor is the method for inclusion of multiple electrons in each theory. The NME formalism is a semiclassical approximation that includes multiple electrons through the dynamic polarizability of the molecule while the TDHF is a quantum mechanical approach which includes each electron explicitly through the wave function. The second factor is the Stark shifting of the excited states which is affected by the first factor. NME theory is derived starting from a two-state Landau−Zehner avoided crossing which assumes that the minimum energy separation between the ground and doorway state occurs at zero field. TDHF does not make this assumption and does allow for Stark shifting of all the states through relaxation of the molecular orbitals in the electric field. This can result in an energy spacing between the ground and excited state which is smaller than the field free energy spacing, thus increasing the excitation probability as observed in Figure 6.

b. Evolution of Electronic Excitation during the Pulse: Windowed Fourier Transform. A windowed Fourier transform (WFT) can be used to probe the electronic dynamics during interaction of the laser field with a molecule. A typical two-dimensional WFT plot reflecting the time dependence of the overlap of the window with the dipole moment is shown in Figure 7a for the window shifting consecutively over 1700 steps of 12 as in size. The laser pulse parameters used for excitation of CO_2 are $\omega = 0.06$ au, $I_{max} = 1.1 \times 10^{14}$ W/cm^2, fwhm = 3.5 fs, Gaussian envelope, and CEP = 0. The largest feature, at approximately 1.63 eV, is the adiabatic response of the dipole moment due to the polarization of the molecular electrons. Figure 7b shows a magnification of the region from 0 to 35 eV making the salient features visible and also showing the projection in the τ vs ε direction. Figure 7c shows the contour plot of the projection onto the $\Delta\tau$ vs ε plane where $\Delta\tau$ is the delay, in femtoseconds, between the maximum of the window and maximum of the dipole moment (i.e., $\Delta\tau = 0$ indicates maximum overlap).

The photon energy used in this simulation was 1.63 eV ($\omega = 0.06$ au), so the excitation shown in Figure 7c is nonlinear and nonadiabatic. As a first step in investigating the excitation processes, the intensity was varied while the fwhm of the excitation pulse was kept constant at 3.5 fs. Figure 8 shows the results of increasing the intensity from 1.1 to 2.5 to 5.0 $\times 10^{14}$ W/cm^2. The time-dependent excitation profile of Figure 8a reveals that population appears first in the 14.3 eV state. After maximum overlap ($\Delta\tau = 0$) population appears in the 15.7, 12.4, and 16.9 eV states, in that order. The Fourier amplitudes and the order of excited state population are mainly determined by the dipole coupling between the ground and excited states. The excited states with the largest transition dipole moments are the states at 12.4, 14.3, 15.7, and 16.7 eV. The magnitude of the transition dipole moments (d_T) follows the order d_T(14.3 eV) > d_T(15.7 eV) > d_T(12.3 eV) > d_T(16.7 eV), as shown in Table 1. The order of appearance and intensity of a given state in the time-dependent excitation profile correlates well with the relative value of the transition dipole from the ground state.

Analysis of the time-dependent Fourier components (or spectrogram) shown in parts a−c of Figure 8 reveals a nonlinear increase in excitation volume with increasing intensity. This is evident in the intensity-dependent Fourier amplitudes of the 12.4, 14.3, 15.7, and 16.8 eV features analyzed after the maximum of laser intensity where each of these peaks reaches its respective maximum. At an intensity of 1.1 $\times 10^{14}$ W/cm^2, Figure 8a, the approximate amplitudes of these four peaks are 0.012, 0.025, 0.02, and 0.01, respectively. As the excitation intensity is doubled to $I = 2.5 \times 10^{14}$ W/cm^2, shown in Figure 8b, the approximate amplitudes of the 14.3, 15.7, 12.3, and 16.7 eV states increase to 0.25, 0.11, 0.14, and 0.12, respectively. The Fourier amplitudes have increased roughly an order of magnitude after doubling the laser intensity, consistent with nonadiabatic excitation as shown in eq 7 and Figure 6. If the Fourier amplitude scale in Figure 8b is reduced to 0.10, it is readily

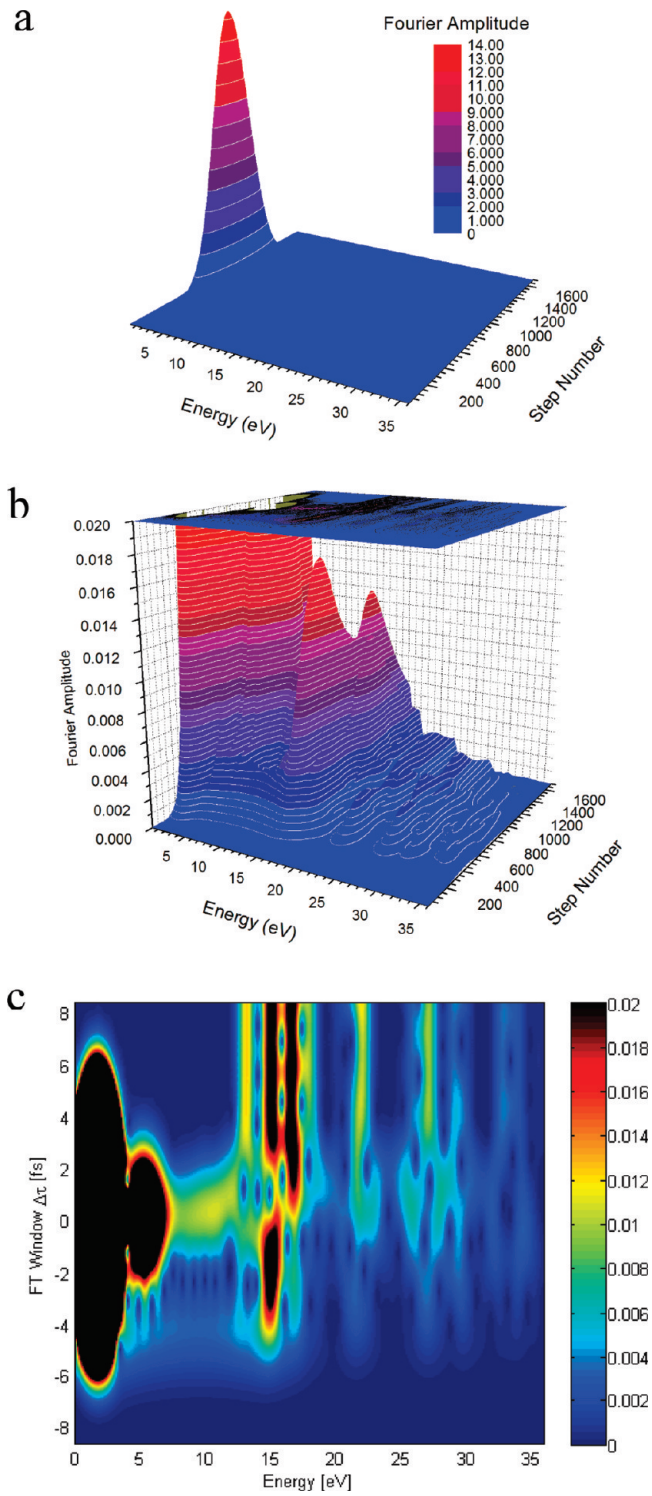

Figure 7. The windowed Fourier transform for $\omega = 0.06$ au, $I = 1.1 \times 10^{14}$ W/cm^2 and step size of 12 as for (a) the full scale Fourier amplitude, (b) a maximum Fourier amplitude of 0.02 revealing small amplitude structure, and (c) the contour plot of (b).

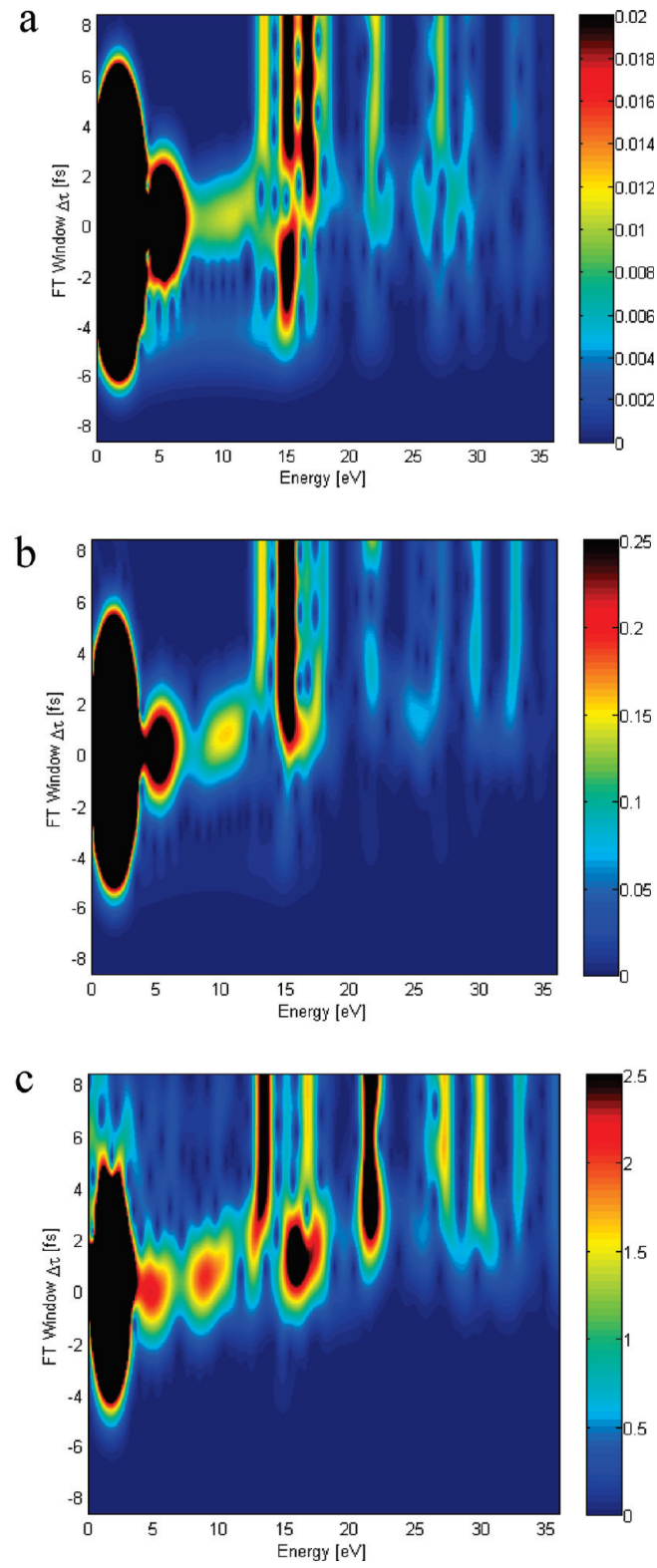

Figure 8. Contour plots of the windowed Fourier transform for $\omega = 0.06$ au with a step size of 12 as for intensities of (a) $I = 1.1 \times 10^{14}$ W/cm^2, (b) 2.5×10^{14}, and (c) 5.0×10^{14} W/cm^2.

apparent that population appears in the 14.7 eV state early in the overlap and population appears in the 15.7 eV state before $\Delta t = 0$. Figure 8c, corresponds to an intensity of $I = 5.0 \times 10^{14}$ W/cm^2. At this intensity the 12.4 and 20.8 eV states have the largest Fourier amplitudes. Decreasing the Fourier amplitude scale to 0.10 again reveals that population appears in the 14.eV state first at approximately $\Delta t = -5.5$ fs. Population in excited states, other than the 14 and 12.4 eV states, does not appear until after $\Delta t = 0$.

Figure 8c also shows that there is significant Stark shifting of the 12.4 eV state on the order of $\delta = -0.7$ eV. This -0.7 eV decrease in the state energy shifts the 12.4 eV state into a near 7 ($\sim$7.13) photon resonance. The signature in the excitation spectrum of a state Stark shifted into a multiphoton resonance with the field is populated mainly in the resonant state.[53] In contrast, the signature of nonadiabatic excitation in the excitation

spectrum is a distribution of population over several excited states with transition dipoles connecting them to the ground state.[53] The excitation in this case appears to be nonadiabatic because the population is distributed over several excited states. The 12.4 eV state is a charge transfer state which moves an electron from the oxygen at one end of the CO_2 molecule to the oxygen atom to the other end. The population of the 14.3 eV state appears as a large broad peak due to the Stark shifting of the nearby states (and the resolution of the windowed Fourier transform). The 20.7 eV state has larger Fourier amplitude than both the 14.3 and 15.7 eV states. This is due to the coupling of the 12.4 and 20.7 eV states. The transition dipole between these two excited states is 0.301 au, which results in rapid population transfer from the 12.4 eV state to the 20.7 eV state. The rapid coupling to other states is one characteristic of the doorway state in NME theory. The relative peak heights of the WFT in Figure 8 agree with the relative peak heights of the Fourier transform of the residual dipole moment oscillations shown in Figure 5. The WFT shows that most of the nonlinear excitation takes place at or after the peak of the electric field.

The two features observed at ~5 and ~8.5 eV in Figure 8 have a fundamentally different time dependence than all of the other features in the spectrogram. The Gaussian shape in both the time delay and energy coordinates for the ~5 and ~8.5 eV features indicates a transient process existing only during the laser pulse. Since there are no field-free dipole allowed excited states in the linear response regime at energies of ~5 and ~8.5 eV, these features arise from the adiabatic response of the molecule to the applied field. This can be shown by exploring the response of the ground state dipole moment to the electric field. This removes all nonadiabatic excitation from the instantaneous dipole moment leaving only the adiabatic response. Figure 9a shows the response of the ground state dipole moment for a pulse with $I = 5.0 \times 10^{14}$ W/cm^2, fwhm = 3.5 fs, and a field frequency of $\omega = 0.06$ au. The ~5 and ~8.5 eV features still appear in the WFT suggesting that these features are real and are due to the adiabatic response of the molecule to the applied electric field.

The most important features shown in Figure 9 are the changes in excitation spectra with a change in carrier frequency and increase in pulse duration. In Figure 8a ($\omega = 0.06$ au) the 12.4 eV peak has the largest Fourier amplitude and the 20.7 eV peak has the second largest Fourier amplitude while in Figure 9b ($\omega = 0.0735$ au) the 14.3 eV peak has the largest Fourier amplitude and the amplitudes of the 12.4 and 20.7 eV peaks are not nearly as large as the corresponding peaks in Figure 8a. Increasing the fwhm of the pulse may make the response slightly more adiabatic because the ramping time to the maximum electric field increases making the cycle to cycle changes in E_{max} smaller in comparison with a shorter pulse. Increasing the pulse duration should have a significant effect on the excitation spectrum. Figure 9c shows the results of increasing the pulse duration to from 3.5 to 5.6 fs with the intensity and photon energy of $I = 5.0 \times 10^{14}$ W/cm^2 and 0.06 au, respectively. The excitation spectrum shows significantly more population in higher energy excited states (i.e., 14.3, 15.6, 20.7, 25.6, and ~30 eV states) than the excitation spectrum of Figure 8c. As discussed in section a, this may be the result of changes in the electric field maxima per half cycle since that is the main difference in the electric fields between Figures 8c and 9c.

A simple experiment to demonstrate the degree of nonadiabatic excitation would be to measure the fragmentation distribution as a function of pulse shape for the pulses shown in parts c and d of Figure 3, for example. While the pulse spectrum is identical, the degree of nonadiabaitc excitation is much larger in Figure 3c as revealed in the greater excited state population in Figure 4c in comparison with Figure 4d. The difference is completely due to the phase of the pulse. This should be

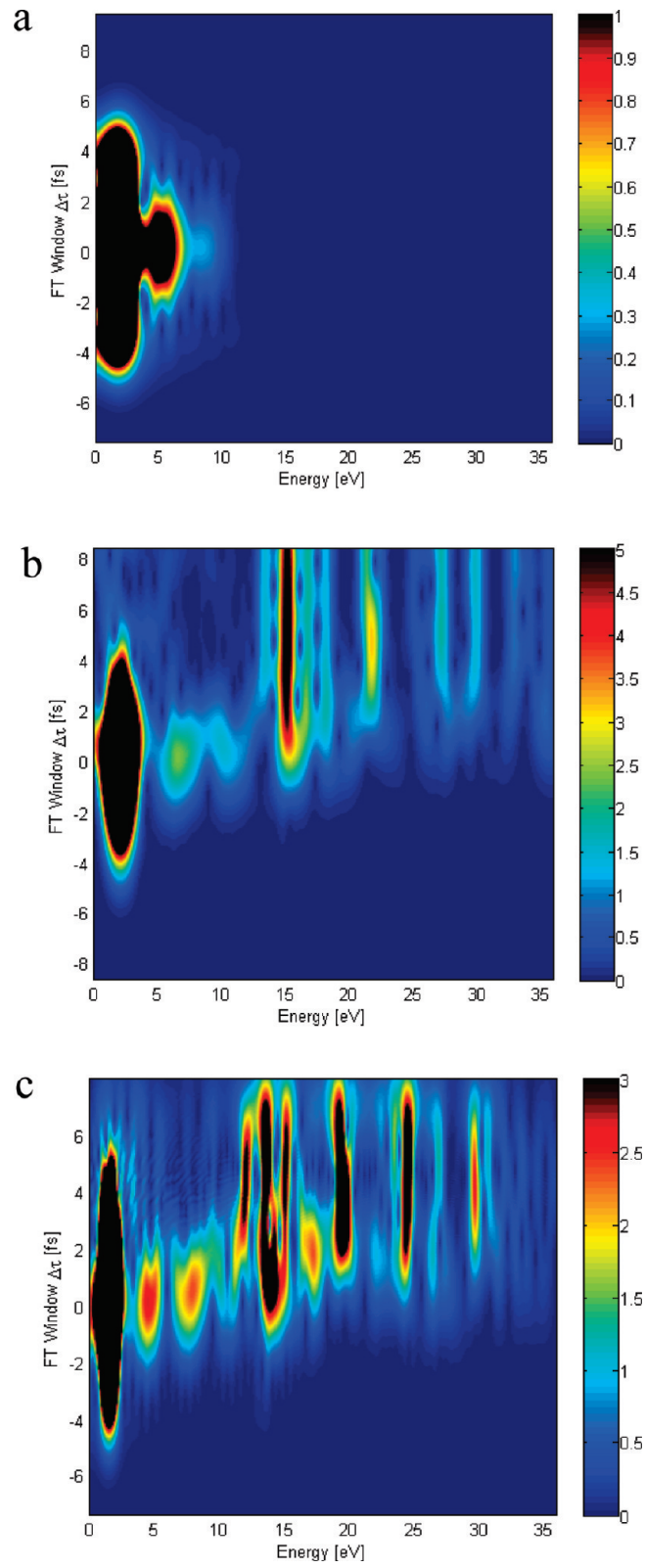

Figure 9. The windowed Fourier transform for a Gaussian pulse with $\varphi = 0°$, $I = 5.0 \times 10^{14}$ W/cm^2, and step size of 12 as (a) showing the adiabatic response of CO_2 to a laser pulse with the dipole coupling removed from the Hamiltonian for $\omega = 0.06$ au, FWHM = 3.5 fs; (b) $\omega = 0.0735$ au, FWHM = 3.5 fs; and (c) FWHM = 5.6 fs, $\omega = 0.06$ au.

reflected in the ionization probability as well as the fragmention distribution. We have shown previously that the degree of nonadiabatic excitation correlates well with both the ionization and fragmentation probability in the series of molecules benzene, naphthalene, anthracene, and tetracene.[51,52] Similar experiments can be performed for the CEP effects, wherein we would predict that the fragmentation distribution in the case of Figure 2, for the trapezoid pulse would be increased for phases of zero and π in comparison with $\pi/2$. We note that considerable care must be taken in the experimental arrangement not to wash out the differences in intensity averaging.[54] as the laser focuses, particularly in the case of shaped pulses.[55]

Summary

The bound state electron dynamics for a linear triatomic molecule, CO_2, interacting with a few cycle pulses reveals that the attosecond dynamics are sensitive to the pulse shape, intensity, carrier envelope phase, ramping time, and total pulse duration. For short pulses on the order of three, or fewer, optical cycles of the field, the effects of the ramping time, total pulse duration, carrier envelope phase, and integrated pulse energy cannot be readily deconvoluted. Each electric field property has an effect on the electric field, $E(t)$, and $E(t)$ determines the excitation spectra. A windowed Fourier transform was used to extract the attosecond electron excitation dynamics during the pulse. The Fourier analysis showed the excitation to contain nonlinear adiabatic and nonadiabatic parts.

Acknowledgment. S.S. and D.R. acknowledge very useful conversations with A. Stolow, O. Smirnova, and M. Ivanov and funding from the National Science Foundation Grant No. CHE0518497 to R.J.L. and CHE0910858 to H.B.S.

References and Notes

(1) Kienberger, R.; Goulielmakis, E.; Uiberacker, M.; Baltuska, A.; Yakovlev, V.; Bammer, F.; Scrinzi, A.; Westerwalbesloh, T.; Kleineberg, U.; Heinzmann, U.; Drescher, M.; Krausz, F. Atomic transient recorder. *Nature* **2004**, *427*, 817.

(2) Paul, P. M.; Toma, E. S.; Breger, P.; Mullot, G.; Auge, F.; Balcou, P.; Muller, H. G.; Agostini, P. Observation of a train of attosecond pulses from high harmonic generation. *Science* **2001**, *292*, 1689.

(3) Mairesse, Y.; de Bohan, A.; Frasinski, L. J.; Merdji, H.; Dinu, L. C.; Monchicourt, P.; Breger, P.; Kovacev, M.; Taieb, R.; Carre, B.; Muller, H. G.; Agostini, P.; Salieres, P. Attosecond synchronization of high-harmonic soft x-rays. *Science* **2003**, *302*, 1540.

(4) Quere, F.; Mairesse, Y.; Itatani, J. Temporal characterization of attosecond XUV fields. *J. Mod. Opt.* **2005**, *53*, 339.

(5) Wickenhauser, M.; Burgdorfer, J.; Krausz, F.; Drescher, M. Time resolved Fano resonances. *Phys. Rev. Lett.* **2005**, *94*, 023002.

(6) Wickenhauser, M.; Burgdorfer, J.; Krausz, F.; Drescher, M. Attosecond streaking of overlapping Fano resonances. *J. Mod. Opt.* **2006**, *53*, 247.

(7) Drescher, M.; Hentschel, M.; Kienberger, R.; Tempea, G.; Spielmann, C.; Reider, G. A.; Corkum, P. B.; Krausz, F. X-ray pulses approaching the attosecond frontier. *Science* **2001**, *291*, 1923.

(8) Jones, R. R.; You, D.; Bucksbaum, P. H. Ionization of Rydberg Atoms by Subpicosecond Half-Cycle Electromagnetic Pulses. *Phys. Rev. Lett.* **1993**, *70*, 1236.

(9) Posthumus, J. H. The dynamics of small molecules in intense laser fields. *Rep. Prog. Phys.* **2004**, *67*, 623.

(10) Baltuska, A.; Udem, T.; Uiberacker, M.; Hentschel, M.; Goulielmakis, E.; Gohle, C.; Holzwarth, R.; Yakoviev, V. S.; Scrinzi, A.; Hansch, T. W.; Krausz, F. Attosecond control of electronic processes by intense light fields. *Nature* **2003**, *421*, 611.

(11) Brabec, T.; Krausz, F. Intense few-cycle laser fields: Frontiers of nonlinear optics. *Rev. Mod. Phys.* **2000**, *72*, 545.

(12) Gurtler, A.; Robicheaux, F.; Vrakking, M. J. J.; van der Zande, W. J.; Noordam, L. D. Carrier phase dependence in the ionization of Rydberg atoms by short radio-frequency pulses: A model system for high order harmonic generation. *Phys. Rev. Lett.* **2004**, *92*, 063901.

(13) Uiberacker, M.; Uphues, T.; Schultze, M.; Verhoef, A. J.; Yakovlev, V.; Kling, M. F.; Rauschenberger, J.; Kabachnik, N. M.; Schroder, H.; Lezius, M.; Kompa, K. L.; Muller, H. G.; Vrakking, M. J. J.; Hendel, S.; Kleineberg, U.; Heinzmann, U.; Drescher, M.; Krausz, F. Attosecond real-time observation of electron tunnelling in atoms. *Nature* **2007**, *446*, 627.

(14) Chelkowski, S.; Bandrauk, A. D.; Apolonski, A. Phase-dependent asymmetries in strong-field photoionization by few-cycle laser pulses. *Phys. Rev. A* **2004**, *70*, 013815.

(15) Apolonski, A.; Poppe, A.; Tempea, G.; Spielmann, C.; Udem, T.; Holzwarth, R.; Hansch, T. W.; Krausz, F. Controlling the phase evolution of few-cycle light pulses. *Phys. Rev. Lett.* **2000**, *85*, 740.

(16) Spielmann, C.; Burnett, N. H.; Sartania, S.; Koppitsch, R.; Schnurer, M.; Kan, C.; Lenzner, M.; Wobrauschek, P.; Krausz, F. Generation of coherent X-rays in the water window using 5-fs laser pulses. *Science* **1997**, *278*, 661.

(17) Christov, I. P. Phase-dependent loss due to nonadiabatic ionization by sub-10-fs pulses. *Opt. Lett.* **1999**, *24*, 1425.

(18) Christov, I. P. Phase-dependent ionization in the barrier suppression regime. *Appl. Phys. B* **2000**, *70*, 459.

(19) Milosevic, D. B.; Paulus, G. G.; Becker, W. High-order above-threshold ionization with few-cycle pulse: a meter of the absolute phase. *Opt. Express* **2003**, *11*, 1418.

(20) Milosevic, D. B.; Paulus, G. G.; Becker, W. Above-threshold ionization with few-cycle laser pulses and the relevance of the absolute phase. *Laser Phys.* **2003**, *13*, 948.

(21) Paulus, G. G.; Lindner, F.; Walther, H.; Baltuska, A.; Goulielmakis, E.; Lezius, M.; Krausz, F. Measurement of the phase of few-cycle laser pulses. *Phys. Rev. Lett.* **2003**, *91*, 253004.

(22) Villoresi, P.; Paulus, G. G.; Grasbon, F.; Walther, H.; Nisoli, M.; Priori, E.; Stagira, S.; Sansone, G.; De Silvestri, S. Absolute phase phenomena induced by few-cycle laser pulses in a strong-field photoionization experiment. *Laser Phys.* **2003**, *13*, 943.

(23) de Bohan, A.; Antoine, P.; Milosevic, D. B.; Piraux, B. Phase-dependent harmonic emission with ultrashort laser pulses. *Phys. Rev. Lett.* **1998**, *81*, 1837.

(24) van der Zwan, E. V.; Lein, M. Control of recollision wave packets for molecular orbital tomography using short laser pulses. *J. Phys. B: At., Mol. Opt. Phys.* **2008**, *41*, 074009.

(25) Milosevic, D. B.; Paulus, G. G.; Becker, W. Phase-dependent effects of a few-cycle laser pulse. *Phys. Rev. Lett.* **2002**, *89*, 153001.

(26) Paulus, G. G.; Grasbon, F.; Walther, H.; Villoresi, P.; Nisoli, M.; Stagira, S.; Priori, E.; De Silvestri, S. Absolute-phase phenomena in photoionization with few-cycle laser pulses. *Nature* **2001**, *414*, 182.

(27) Dietrich, P.; Krausz, F.; Corkum, P. B. Determining the absolute carrier phase of a few-cycle laser pulse. *Opt. Lett.* **2000**, *25*, 16.

(28) Chelkowski, S.; Shon, N. H.; Bandrauk, A. D. Measuring the absolute phase of an ultrashort intense laser pulse. *Laser Phys.* **2003**, *13*, 871.

(29) Chelkowski, S.; Bandrauk, A. D. Sensitivity of spatial photoelectron distributions to the absolute phase of an ultrashort intense laser pulse. *Phys. Rev. A* **2002**, *65*, 061802.

(30) Gurtler, A.; Robicheaux, F.; van der Zande, W. J.; Noordam, L. D. Asymmetry in the strong-field ionization of Rydberg atoms by few-cycle pulses. *Phys. Rev. Lett.* **2004**, *92*, 033002.

(31) Smith, S. M.; Li, X. S.; Markevitch, A.; Romanov, D.; Levis, R. J.; Schlegel, H. B. Numerical simulation of nonadiabatic electron excitation in the strong-field regime. 3. Polyacene neutrals and cations. *J. Phys. Chem. A* **2007**, *111*, 6920.

(32) Smith, S. M.; Li, X. S.; Markevitch, A. N.; Romanov, D. A.; Levis, R. J.; Schlegel, H. B. A numerical simulation of nonadiabatic electron excitation in the strong field regime: Linear polyenes. *J. Phys. Chem. A* **2005**, *109*, 5176.

(33) Smith, S. M.; Li, X. S.; Markevitch, A. N.; Romanov, D. A.; Levis, R. J.; Schlegel, H. B. Numerical simulation of nonadiabatic electron excitation in the strong field regime. 2. Linear polyene cations. *J. Phys. Chem. A* **2005**, *109*, 10527.

(34) Kono, H.; Sato, Y.; Kanno, M.; Nakai, K.; Kato, T. Theoretical investigations of the electronic and nuclear dynamics of molecules in intense laser fields: Quantum mechanical wave packet approaches. *Bull. Chem. Soc. Jpn.* **2006**, *79*, 196.

(35) Kono, H.; Sato, Y.; Tanaka, N.; Kato, T.; Nakai, K.; Koseki, S.; Fujimura, Y. Quantum mechanical study of electronic and nuclear dynamics of molecules in intense laser fields. *Chem. Phys.* **2004**, *304*, 203.

(36) Sato, Y.; Kono, H.; Koseki, S.; Fujimura, Y. Description of molecular dynamics in intense laser fields by the time-dependent adiabatic state approach: Application to simultaneous two-bond dissociation of CO2 and its control. *J. Am. Chem. Soc.* **2003**, *125*, 8019.

(37) Li, X. S.; Smith, S. M.; Markevitch, A. N.; Romanov, D. A.; Levis, R. J.; Schlegel, H. B. A time-dependent Hartree-Fock approach for studying the electronic optical response of molecules in intense fields. *Phys. Chem. Chem. Phys.* **2005**, *7*, 233.

(38) Frisch, M. J.; Trucks, G. W.; Schlegel, H. B.; Scuseria, G. E.; Robb, M. A.; Cheeseman, J. R.; Montgomery, J. A., Jr.; Vreven, T.; Kudin, K. N.; Burant, J. C.; Millam, J. M.; Iyengar, S. S.; Tomasi, J.; Barone, V.; Mennucci, B.; Cossi, M.; Scalmani, G.; Rega, N.; Petersson, G. A.;

Nakatsuji, H.; Hada, M.; Ehara, M.; Toyota, K.; Fukuda, R.; Hasegawa, J.; Ishida, M.; Nakajima, T.; Honda, Y.; Kitao, O.; Nakai, H.; Klene, M.; Li, X.; Knox, J. E.; Hratchian, H. P.; Cross, J. B.; Bakken, V.; Adamo, C.; Jaramillo, J.; Gomperts, R.; Stratmann, R. E.; Yazyev, O.; Austin, A. J.; Cammi, R.; Pomelli, C.; Ochterski, J. W.; Ayala, P. Y.; Morokuma, K.; Voth, G. A.; Salvador, P.; Dannenberg, J. J.; Zakrzewski, V. G.; Dapprich, S.; Daniels, A. D.; Strain, M. C.; Farkas, O.; Malick, D. K.; Rabuck, A. D.; Raghavachari, K.; Foresman, J. B.; Ortiz, J. V.; Cui, Q.; Baboul, A. G.; Clifford, S.; Cioslowski, J.; Stefanov, B. B.; Liu, G.; Liashenko, A.; Piskorz, P.; Komaromi, I.; Martin, R. L.; Fox, D. J.; Keith, T.; Al-Laham, M. A.; Peng, C. Y.; Nanayakkara, A.; Challacombe, M.; Gill, P. M. W.; Johnson, B.; Chen, W.; Wong, M. W.; Gonzalez, C.; Pople, J. A. *Gaussian Development Version, Revision. d01p*; Gaussian, Inc.: Wallingford, CT, 2006.

(39) Kendall, R.; Dunning, T. H.; Harrison, R. J. *J. Chem. Phys.* **1992**, *96*, 6796.

(40) Woon, D. E.; Dunning, T. H. *J. Chem. Phys.* **1993**, *98*, 1358.

(41) Winter, N. W.; Bender, C. F.; Goddard, W. A. Theoretical Assignments of Low-Lying Electronic States of Carbon Dioxide. *J. Chem. Phys.* **1973**, *20*, 480.

(42) Resch, K.; Blanchet, V.; Stolow, A.; Seideman, T. Toward polyatomic wave packet decomposition: Final state effects. *J. Phys. Chem. A* **2001**, *105*, 2756.

(43) Vrakking, M. J. J.; Villeneuve, D. M.; Stolow, A. Observation of fractional revivals of a molecular wave packet. *Phys. Rev. A* **1996**, *54*, R37.

(44) Hunter, E. P.; Lias, S. G. Gas phase ion energetics. In *NIST Chemistry WebBook*; Linstrom, P. J., Mallard, W. G., Eds.; NIST Standard Reference Database Number 69; National Institute of Standards and Technology: Gaithersburg, MD.

(45) Smirnova, O.; Mouritzen, A. S.; Patchkovskii, S.; Ivanov, M. Y. Coulomb-laser coupling in laser-assisted photoionization and molecular tomography. *J. Phys. B: At., Mol. Opt. Phys.* **2007**, *40*, F197.

(46) Smirnova, O.; Spanner, M.; Ivanov, M. Analytical solutions for strong field-driven atomic and molecular one- and two-electron continua and applications to strong-field problems. *Phys. Rev. A* **2008**, *77*, 033407.

(47) Smirnova, O.; Spanner, M.; Ivanov, M. Y. Coulomb and polarization effects in laser-assisted XUV ionization. *J. Phys. B: At., Mol. Opt. Phys.* **2006**, *39*, S307.

(48) Okabe, H. *Photochemistry of small molecules*; Wiley: New York, 1978.

(49) Lezius, M.; Blanchet, V.; Ivanov, M. Y.; Stolow, A. Polyatomic molecules in strong laser fields: Nonadiabatic multielectron dynamics. *J. Chem. Phys.* **2002**, *117*, 1575.

(50) Lezius, M.; Blanchet, V.; Rayner, D. M.; Villeneuve, D. M.; Stolow, A.; Ivanov, M. Y. Nonadiabatic multielectron dynamics in strong field molecular ionization. *Phys. Rev. Lett.* **2001**, *86*, 51.

(51) Markevitch, A. N.; Romanov, D. A.; Smith, S. M.; Schlegel, H. B.; Ivanov, M. Y.; Levis, R. J. Sequential nonadiabatic excitation of large molecules and ions driven by strong laser fields. *Phys. Rev. A* **2004**, *69*, 013401.

(52) Markevitch, A. N.; Smith, S. M.; Romanov, D. A.; Schlegel, H. B.; Ivanov, M. Y.; Levis, R. J. Nonadiabatic dynamics of polyatomic molecules and ions in strong laser fields. *Phys. Rev. A* **2003**, *68*, 011402.

(53) Smith, S. M.; Romanov, D.; Heck, T. J.; Schlegel, H. B.; Levis, R. J. Observing the transition from Stark-Shifted, strong-field resonant to nonadiabatic excitation, *J. Phys. Chem. A*, in press.

(54) Walker, B.; Sheehy, B.; Dimauro, L. F.; Agostini, P.; Schafer, K. J.; Kulander, K. C. Precision-Measurement of Strong-Field Double-Ionization of Helium. *Phys. Rev. Lett.* **1994**, *73*, 1227.

(55) Sussman, B. J.; Lausten, R.; Stolow, A. Focusing of light following a 4-f pulse shaper: Considerations for quantum control. *Phys. Rev. A* **2008**, *77*, 043416.

JP904549D